Case Studies of the Impact of Orbital Sampling on Stratospheric Trend Detection and Derivation of Tropical Vertical Velocities: Solar Occultation versus Limb Emission Sounding

Luis F. Millán[1], Nathaniel J. Livesey[1], Michelle L. Santee[1], Jessica L. Neu[1], Gloria L. Manney[2,3], and Ryan A. Fuller[1]

[1]Jet Propulsion Laboratory, California Institute of Technology, Pasadena, California, USA
[2]New Mexico Institute of Mining and Technology, USA
[3]NorthWest Research Associates, USA

Correspondence to: L. Millán (luis.f.millan@jpl.nasa.gov)

Abstract. This study investigates the representativeness of two types of orbital sampling applied to stratospheric temperature and trace gas fields. Model fields are sampled using real sampling patterns from the Aura Microwave Limb Sounder (MLS), the HALogen Occultation Experiment (HALOE) and the Atmospheric Chemistry Experiment Fourier Transform Spectrometer (ACE-FTS). The MLS sampling acts as a proxy for a dense uniform sampling pattern typical of limb emission sounders, while HALOE and ACE-FTS represent coarse non-uniform sampling patterns characteristic of solar occultation instruments. First, this study revisits the impact of sampling patterns in terms of the sampling bias, as previous studies have done. Then, it quantifies the impact of different sampling patterns on the estimation of trends and their associated detectability. In general, we find that coarse non-uniform sampling patterns may introduce non-negligible errors in the inferred magnitude of temperature and trace gas trends and necessitate considerably longer records for their definitive detection. Lastly, we explore the impact of these sampling patterns on tropical vertical velocities derived from stratospheric water vapor measurements. We find that coarse non-uniform sampling may lead to a biased depiction of the tropical vertical velocities and, hence, to a biased estimation of the impact of the mechanisms that modulate these velocities. These case studies suggest that dense uniform sampling such as that available from limb emission sounders provides much greater fidelity in detecting signals of stratospheric change (for example, fingerprints of greenhouse gas warming and stratospheric ozone recovery) than coarse non-uniform sampling such as that of solar occultation instruments.

1 Introduction

Satellite data have provided a wealth of information on the Earth system and have had a profound impact on operational numerical weather forecasting. Unlike ground-based instruments or airborne field campaigns, satellite data provide continuous global coverage, which facilitates the study and assimilation of distributions of atmospheric fields, as well as global model evaluation. However, satellite measurements sample continuously changing atmospheric fields only at discrete times and locations, depending on the satellite orbit as well as the measurement technique, which can result in a biased depiction of the atmospheric field.

Typically, the impact of orbital sampling has been evaluated by comparing a raw model field against a satellite-sampled one. For example, many studies have documented sampling errors for rainfall estimates (e.g., McConnell and North, 1987; North et al., 1993; Bell and Kundu, 1995; Soman et al., 1996; Gebremichael and Krajewski, 2005), and brightness temperatures (Engelen et al., 2000; Brindley and Harries, 2003), as well as O_3, CO, temperature and a few other atmospheric parameters sampled by nadir-viewing instruments (Luo et al., 2002; Aghedo et al., 2011; Guan et al., 2013). Recently, Toohey et al. (2013) evaluated the sampling bias in monthly and annual mean climatologies of O_3 and H_2O from 16 satellite instruments, including limb emission sounders, limb scattering sounders, solar occultation instruments and a stellar occultation instrument. They concluded that coarse sampling may introduce significant sampling uncertainties in climatologies, not only through non-uniform spatial sampling but, more importantly, through non-uniform temporal sampling, that is to say, producing regional monthly means using measurements that do not cover the entire month. As expected, the sampling bias was found to be the greatest in regions with large natural variability.

In this study we further evaluate the impact of the Aura Microwave Limb Sounder (MLS), the HALogen Occultation Experiment (HALOE) and the Atmospheric Chemistry Experiment Fourier Transform Spectrometer (ACE-FTS) sampling patterns using the Canadian Middle Atmosphere Model (CMAM). MLS sampling provides a dense uniform pattern, while HALOE and ACE-FTS are representative of coarser solar occultation sampling patterns. We use HALOE and ACE-FTS sampling patterns because they are commonly used solar occultation datasets and, furthermore, because their sampling patterns are significantly different, and thus representative of the range of observation patterns obtained by solar occultation instruments.

Our study has two purposes: (1) We expand upon previous studies by quantifying the sampling bias of these instruments affecting measurements of upper tropospheric and stratospheric temperature and trace gas species. (2) We investigate how differences in data coverage may affect the outcome of two illustrative atmospheric studies: trend detection and quantification of tropical vertical velocities. We assess the differences in the long-term ($>$30 years) trends in temperature, O_3, and CO estimated using datasets with different sampling patterns. Also, we characterize the impact of orbital sampling on derived lower stratospheric tropical vertical velocities. These velocities are computed by correlating the lag of the water vapor “tape recorder” signal between adjacent levels (Niwano et al., 2003; Flury et al., 2012; Jiang et al., 2015). As such, they are likely an upper bound on the actual velocity (Schoeberl et al., 2008). These vertical velocities are modulated by the Quasi-Biennial Oscillation (QBO), seasonal cycles, and El Niño Southern Oscillation (ENSO) (e.g., Flury et al., 2013; Neu et al., 2014; Minschwaner et al., 2016).

This paper is organized as follows: Section 2 describes the satellite patterns and the model fields used. Section 3 briefly revisits sampling bias estimates, while the impact of sampling on the estimation of long-term trends as well as on trend detection is presented in section 4. Section 5 addresses the impact of orbital sampling on derived tropical vertical velocities, and section 6 summarizes our results. The results discussed in this study should be considered as example cases. Whether the results shown represent reasonable estimates of the true orbital sampling induced artifacts (e.g. in the sampling bias, in the inferred magnitude of the trends, or in the derived tropical vertical velocities) may also depend on how well the model fields represent the real atmosphere.

2 Data and Methodology

2.1 Model Fields

CMAM is used as a proxy for the real atmosphere. CMAM is an extension of the Canadian Center for Climate Modeling and Analysis spectral general circulation model. Detailed descriptions of its dynamical and chemical schemes are given by Beagley et al. (1997) and de Grandpré et al. (2000), respectively. The free-running version of the model has been extensively evaluated, and has been shown to agree relatively well with observations relevant to chemistry, dynamics, transport, and radiation (e.g., de Grandpré et al., 2000; Eyring et al., 2006; Hegglin and Shepherd, 2007; Melo et al., 2008; Jin et al., 2005, 2009).

In this study we use output from the CMAM30 Specified Dynamics (SD) simulation in which temperature and winds have been nudged to the ERA-Interim reanalysis. This data set exploits the vast progress made by reanalyses in representing the stratospheric circulation (e.g., Dee et al., 2011) and as such can be used to reliably predict the chemical fields. Before nudging the temperature fields, a technique described by McLandress et al. (2014) was used to remove temporal discontinuities in the ERA-Interim upper stratospheric temperatures that occurred in 1985 and 1998. CMAM30-SD has been shown to have a good representation of stratospheric temperature, O_3, H_2O and CH_4 (Pendlebury et al., 2015), it has been used as a transfer function between satellite datasets to construct a reliable long-term H_2O data record (Hegglin et al., 2014), and it has been shown to reproduce halogen-induced mid-latitudes O_3 loss sufficiently well for investigation of long-term O_3 trends (Shepherd et al., 2014). The version of CMAM30-SD used here has a horizontal resolution of approximately 3.75° latitude by 3.75° longitude. This resolution (approximately 400 km) is comparable to the horizontal resolution of HALOE, ACE-FTS and MLS, which is limited by the $\sim$500 km limb-viewing path length, and, hence, no smoothing of the model fields is necessary (Toohey et al., 2013). This version has 63 vertical levels up to 0.0007 hPa with a vertical resolution varying from 100 m in the lower troposphere to about 3 km in the mesosphere. Model results for the period between January 1979 and December 2012 are used in this study.

We evaluate the following CMAM30-SD outputs: temperature, O_3, CH_3Cl, H_2O, CO, HCl, N_2O, and HNO_3. These parameters are an intersection of the available CMAM30-SD outputs, the measurements available for MLS, and the measurements available for ACE-FTS or HALOE.

2.2 Satellite Instrument Sampling Patterns

In this study we analyze the representativeness of the orbital sampling of the solar occultation instruments HALOE and ACE-FTS, as well as the limb emission sounder MLS. Solar occultation data are extremely valuable for atmospheric studies due to their fine vertical resolution, the excellent precision and accuracy of their self-calibrated measurements, and their potential for detecting many species. However, the sparsity of the measurements makes understanding the impact of their sampling crucial.

HALOE was launched on the Upper Atmosphere Research Satellite (UARS) in 1991, and it measured infrared spectra across eight broadband and gas filter channels from 2.45 μm to 10.04 μm for 14 years. It measured vertical profiles of temperature, pressure and several atmospheric trace gases, with as many as 15 sunrise and 15 sunset profiles of these atmospheric parameters observed at a given latitude each day (Russell et al., 1993). The HALOE sampling sweeps through its full range of latitude coverage, ranging from $\pm 80^o$ to $\pm 50^o$ depending on the season, over a period of about a month. The vertical resolution of this dataset is about 2-3 km.

ACE-FTS was launched in 2003 and profiles the atmosphere by using solar occultation. It measures infrared spectra from 2.2 to 13.3 μm (750 to 4400 cm^{-1}) with high spectral sampling (0.02 cm^{-1}), which allows retrieval of temperature, pressure and concentration for several dozen atmospheric trace gases (Bernath et al., 2005). ACE-FTS is focused on high-latitude science, and thus almost 50% of its approximately 15 sunrise and 15 sunset occultations per day occur at latitudes around 60^o. Global latitude coverage is achieved over a period of approximately three months. The vertical resolution of this dataset is about 3 km.

Aura MLS was launched in 2004 and measures limb millimeter and submillimeter atmospheric thermal emission using heterodyne radiometers covering spectral regions near 118, 191, 240, 640 GHz and 2.5 THz, from which temperature, trace gas concentrations and cloud ice are retrieved. Daily, it covers latitudes from 82^oS to 82^oN with $\sim$3500 vertical scans providing near-global observations. The vertical resolution of this dataset varies among species; O_3, H_2O and HCl have a $\sim$3 km resolution in the stratosphere, and CO, CH_3Cl, HNO_3 and N_2O have a 4–8 km resolution in the stratosphere (Livesey et al., 2015).

To investigate the impact of orbital sampling, the daily model fields are linearly interpolated to the actual latitude and longitude of the satellite measurements. For the sampling patterns, we use a typical year of measurement locations. In particular, we use 1994 and 2005 for HALOE and ACE-FTS, respectively; these are the years with the maximum number of measurements on record for each dataset. For MLS, we use 2008 as a representative year. Gaps in the measurements due to instrument problems as well as year-to-year variations due to orbital state changes are not considered in this study. To avoid differences attributed purely to diurnal cycles, all satellite measurements are assumed to be made at 12UT, obviating the need for interpolation in time. Thus, we focus on spatial differences. Given that our focus is on horizontal/temporal sampling, all satellite measurements are assumed to have vertical resolution comparable to that of CMAM30-SD; however, we want to emphasize that the vertical resolution of these instruments is in general good enough to resolve the model fields. That is, although the impact of the averaging kernels is not addressed in this study, for the parameters studied here a 3 km averaging kernel does not significantly affect their values in the upper troposphere/stratosphere.

Figure 1 (left) shows monthly sampling counts for each instrument. MLS has a dense and nearly uniform sampling over latitude and time, while HALOE and ACE-FTS have sparser and less uniform sample densities because they are limited to two measurements per orbit. Figure 1 (right) shows the zonal mean water vapor field at 100 hPa as sampled by each instrument to highlight how much daily variability may be missed by the HALOE and ACE-FTS sampling patterns. The consequences of these contrasting sampling densities are the main motivation for this study. As discussed by Manney et al. (2007), mapping data into vortex-centered coordinate systems such as those based on potential vorticity (PV) or equivalent latitude (EqL) may alleviate some of the solar occultation sampling density problems for polar processing studies. However, since this study focuses on near-global trends and tropical upwelling velocities, such vortex-centered coordinate systems are of very limited utility here.

3 Sampling Biases

We evaluate the sampling biases associated with constructing monthly zonal means from the raw and satellite-sampled data. The raw or sampled zonal means for a particular latitude bin for each pressure level are given by

$$\overline{Z_l^x} = \frac{1}{N}\sum y_l^x \tag{1}$$

where N is the total number of points, y, belonging to a latitude bin l, and x is a placeholder variable for either the raw data, denoted by the superscript r, or the sampled data, denoted by the superscript s. Figure 2 shows examples of raw and sampled zonal means for temperature, O_3 and H_2O. The difference between the satellite-sampled zonal mean and the raw zonal mean gives the absolute sampling bias, that is to say,

$$S_A = \overline{Z_l^s} - \overline{Z_l^r} \tag{2}$$

or, in percentage,

$$S_P = \frac{\overline{Z_l^s} - \overline{Z_l^r}}{\overline{Z_l^r}} \times 100. \tag{3}$$

Figure 3 shows examples of the sampling biases for temperature, O_3 and H_2O for January 2005 CMAM30-SD fields. Relative biases are shown for trace gas species to accommodate their strong vertical gradients. These biases only display the impact of sampling the CMAM30-SD fields; as mentioned before, how well these biases represent the true atmospheric sampling biases will depend on how close the model fields are to the real atmospheric state.

For each month, instrument, and pressure level, this bias was computed for all the latitude bins in which an instrument was able to sound the atmosphere. To summarize the potential sampling biases we computed root-mean-square (RMS) biases over one year's worth of data. As an example, Figure 4 shows these calculated RMS sampling biases for temperature, O_3 and H_2O for 2005. Overall, there is a direct correlation between the sampling biases and the variability of the geophysical parameters. For example, as noted by Toohey et al. (2013), O_3 sampling biases for the three instruments are smaller in the tropics and larger at midlatitudes and in the polar regions, where variability is low/high, respectively. However, the biases in all regions are minimized by dense uniform sampling such as that of MLS.

Figure 5 shows the mean and maximum sampling biases over all latitudes for the model year 2005 for all the atmospheric parameters studied. In general, HALOE and ACE-FTS sampling patterns produce mean and maximum sampling biases an order of magnitude larger than those of MLS. For example, for the occultation sensors, the temperature maximum sampling biases are about 10 K compared to 1 K for MLS. Similarly, in the middle stratosphere, H_2O maximum sampling biases for the solar occultation instruments can be as large as 5 % compared to less than 1 %, and lastly, HNO_3 maximum sampling biases can be as large as 50 % compared to less than 5 %.

4 Long-Term Trends

We now evaluate the impact of orbital sampling on the representation of long-term trends. Accurate representation of long-term trends is crucial because they are indicators of climate change, as well as ozone recovery. To summarize the effect of the orbital sampling upon long-term trends we use Taylor diagrams (Taylor, 2001), which provide a convenient method for visualizing statistics of how closely patterns match each other; in this case, they are used to depict the success of the satellite-sampled data in representing the variability found in the raw model fields. The similarity is quantified by their correlation coefficient, their centered RMS difference (RMSd) and their standard deviations. Simply, the centered RMSd is the RMS of the differences between the two anomaly time series.

In the diagrams shown, all data are normalized to the raw-model standard deviation to facilitate showing different pressure levels in the same figure. In these diagrams, there are four things to consider: (1) the azimuth angle indicates the correlation between the satellite-sampled and raw data, (2) the point with normalized standard deviation of one and correlation of one is the reference point and corresponds to the raw model data, (3) the distance between any point in the figure and the reference point indicates the ratio of the centered RMSd and the raw-model standard deviation (green contours), and (4) the distance between other points in the plot and the origin is the ratio between the satellite-sampled standard deviation and that of the raw model field.

Near-global (60°S-60°N) long-term (1979–2012) patterns are compared between satellite-sampled and raw model fields in Figure 6 for all the atmospheric parameters evaluated in this study. Means were computed by averaging all data available between 60°N and 60°S with no effort to use only latitudes where the satellites sampled. This approach was taken to show the representativeness of near-global patterns. We did not expand this study to the latitudes poleward of 60°N or 60°S because ACE-FTS does not sample these areas for four months per calendar year and HALOE does not sample for 5 and 6 months at the South and North Pole, respectively (see Figure 1). Figure 7 shows the raw model standard deviations used to normalize these diagrams (black lines). Overall, the MLS-sampled data (circles in Figure 6) for all variables and all pressure levels are close to the reference point, indicating high correlation coefficients, low centered RMSd and the expected standard deviation (i.e., a standard deviation similar to that of the full model fields). The HALOE-sampled data (triangles) show intermediate performance, followed by the ACE-FTS-sampled data (squares), which show the weakest correlation and the largest normalized standard deviation. For example, this is easily seen in the CO Taylor diagram, where the MLS-sampled points all cluster tightly at the reference point, whereas HALOE-sampled points lie farther away and ACE-FTS-sampled points the farthest.

To highlight the impact of these sampling differences, Figure 8 shows trend estimates for near-global temperature at 10 hPa using the raw and satellite-sampled data. Three methods have been used to compute the trends. The first is a simple linear fit (an ordinary least square regression) through the points. In the second, we deseasonalize the data (we remove the observed climatological monthly mean at every grid point) before computing a linear fit. Lastly, we consider a trend model of the form,

$$Y = \mu + \omega \frac{t}{12} + S + N \tag{4}$$

where Y are the monthly raw or sampled average measurements (temperature, CO or O_3 concentration, etc), μ is a baseline constant, ω is the mean trend per year, t is time in months, S is a seasonal mean component represented by

$$S = a_1 sin(\frac{2\pi}{12}t + b_1) + a_2 sin(\frac{2\pi}{6}t + b_2) \tag{5}$$

and N is the unexplained portion of the data assumed to follow a first order autoregressive model [AR(1)]. That is, it satisfies

$$N = \phi N_1 + \varepsilon \tag{6}$$

where ϕ is the autocorrelation of the noise, computed, and assumed temporally invariant, following Tiao et al. (1990), and ε are independent white noise variables with variance σ_ε^2. As pointed out by Tiao et al. (1990), ϕ has the effect of reducing the amount of information that would have been available in the same number of independent data points. Similar models have been used in many previous trend studies (e.g. Tiao et al., 1990; Weatherhead et al., 1998; Boers and Meijgaard, 2009; Whiteman et al., 2011). As shown in Figure 8, HALOE (ACE-FTS) sampling artificially reduces (increases) the trend estimates by about 10% (25%). Despite agreement on the sign of the trend, these sampling-induced artifacts will compromise the robustness of the derived temperature trends. We computed the trend using different methods in order to emphasize that using models that are more geophysically realistic, such as those that capture the seasonal component, may not have much impact on the estimated trends, or, as pointed out by Weatherhead et al. (1998), on the trend statistical properties.

Figure 9 shows how these sampling-induced trend artifacts vary with altitude. To avoid clutter, this figure only shows the differences in trend magnitude computed using equation 4, but the ones computed using the other trend detection methods are similar. We show results for temperature, O_3 and CO because these parameters exhibit clear trends at most pressure levels in the CMAM30-SD simulations and also because overall they can be accurately described by the model given by equation 4. For O_3 we only use data starting from 2000 to capture the expected period of O_3 recovery. Overall, MLS sampling allows estimation of the trend magnitudes to about an order of magnitude better than HALOE and ACE-FTS sampling, with accuracy better than 1% at most pressure levels for temperature and CO, and better than 10% for O_3.

Figure 9 also shows the estimated number of years required to definitively detect these trends. When using equation 4, the number of years, n^*, needed to detect a given trend with a 95% confidence level with probability of 0.90 can be approximated by (Tiao et al., 1990),

$$n^* = \left[\frac{3.3\sigma_N}{|\omega|}\sqrt{\frac{1+\phi}{1-\phi}}\right]^{2/3} \tag{7}$$

which indicates that trend detectability depends on three factors: (1) ϕ the autocorrelation of the residual between the data points and the trend model computed following Tiao et al. (1990), (2) σ_N the standard deviation of the residual, which corresponds to the unexplained variability of the data, and (3) the absolute magnitude of the trend. It is also noted that σ_N is related to σ_ε by

$$\sigma_N^2 = \frac{\sigma_\varepsilon^2}{1-\phi^2} \tag{8}$$

in this trend model (equation 4). Note that ϕ was computed for the raw as well as the satellite-sampled data. As shown in Figure 9, trend detection using data with HALOE or ACE-FTS sampling will require considerably more years than using data with MLS sampling. This is due to an increase in the magnitude of σ_N resulting from the noisiness of the time series based on the HALOE or ACE-FTS sampling patterns (e.g. Figure 8). For example, at 1 hPa, the pressure level where the strongest temperature trend is found in CMAM30-SD, a 15-year record of MLS-sampled observations would be required to detect such a trend at the 95% confidence level, while HALOE and ACE-FTS sampling would require 25 and 30 years, respectively. For O_3 at 2 hPa, the pressure level where the strongest O_3 trend is found in CMAM30-SD, the MLS sampling pattern would require about 11 years, while HALOE and ACE-FTS would require about 20 and 30 years, respectively. In addition, MLS sampling requires the same number of years as for the raw model fields; that is, the required number of years is only determined by the natural variability. We also performed this analysis using only the autocorrelation computed for the raw model data and found no significant differences.

We also investigated the effect of instrument noise, using Tiao et al. (1990) and Whiteman et al. (2011)

$$\sigma_N = \sqrt{\frac{\sigma_\varepsilon^2}{1-\phi^2} + \frac{\sigma_I^2}{n_I}} \tag{9}$$

where σ_I is the instrument noise and n_I is the number of measurements averaged. Typical noise estimates were taken from Livesey et al. (2015) for MLS; Clerbaux et al. (2005), Sica et al. (2008), and Dupuy et al. (2009) for ACE-FTS; and Hervig et al. (1996) and Brühl et al. (1996) for HALOE. Since HALOE does not measure CO, we assumed the same error as given by Clerbaux et al. (2005) for ACE-FTS. The effect of instrument noise was found to be negligible due to the high number of measurements even for HALOE and ACE-FTS (in a given month, around 70000 for MLS, 600 for HALOE and 270 for ACE-FTS). These estimates of the length of the measurement record required to detect trends do not take into account the effects of a disruption of the measurements for a given period or aging of the instrument, both of which can induce artificial trends in the data that are not representative of the actual environmental trend studied.

Both HALOE and ACE-FTS provide better coverage in the extratropics than in the tropics (see Figure 1). Figure 10 therefore shows long-term pattern comparisons between satellite-sampled and raw data for trends derived using only data from 30° N to 60° N. Figure 7 also shows the raw model standard deviations used to normalize these diagrams (purple lines). In general, HALOE and ACE-FTS sampled data correlation coefficients improved considerably over the near-global case, with correlation coefficient no smaller than $\sim$0.6 and with centered RMSd better than one raw model standard deviation (see Figure 10). MLS-sampled data are still closest to the reference point. Two variables can have similar trends but still perform poorly in Taylor diagrams due to either a lack of correlation or different standard deviations. In both cases, this will impact σ_N, resulting in an increase in the number of years required to statistically detect such a trend.

Figure 11 is equivalent to Figure 9 but for the 30° N to 60° N latitude range. As for the near-global trends, ACE-FTS sampling still requires considerably more years to confidently detect a trend than does MLS sampling. HALOE, however, has a more uniform sampling density than ACE-FTS in this latitude range (see Figure 1), and thus the time required to detect a trend is more in line with that for MLS. Nevertheless, MLS sampling allows estimation of trends to about an order of magnitude better than HALOE and ACE-FTS sampling. As before, the effect of instrument noise was found to be negligible (for this latitude range the approximate number of measurements in a given month is 19000, 220 and 70 for MLS, HALOE and ACE-FTS, respectively).

As shown, the ability to detect trends depends upon the natural variability and the correlation of the data. These in turn vary with the specific parameter as well as the location and height being studied. Studies of natural variability and autocorrelation of the data will help identify where to monitor to find more readily detectable trends, but such a study is outside the scope of this paper.

5 Tropical Vertical Velocities

In this section we investigate the impact of orbital sampling upon derived tropical vertical velocities (a key metric for atmospheric circulation). The vertical velocities are calculated using the same approach as described by Flury et al. (2012) and Jiang et al. (2015). In short, we use time series of daily zonal mean water vapor data averaged between 8°S and 8°N (see Figure 12). We correlate these time series at different pressure levels and determine the time lag for the best correlation. The vertical velocity for the midpoint of each layer is simply computed by dividing the distance between the pressure levels (the altitude difference) by the lag. These calculations were performed using the raw model CMAM30-SD simulations as well as the satellite-sampled data. The vertical velocities derived from this method are a measure of the transport velocity averaged over 8°S-8°N and have been shown to agree well with the Transformed Eulerian Mean residual vertical velocity when in-mixing from the extratropics and vertical diffusion are small (Schoeberl et al., 2008). Interpolation was used to fill the data gaps due to the sampling patterns. In the case of HALOE sampling, this implies linearly interpolating to fill gaps in June and December. For ACE-FTS gaps are filled in January, March, May, July, September, November and December, when no measurements are made over the tropics (8°S to 8°N); thus, we are applying the analysis to highly interpolated data. Considering the degree of interpolation required, we do not recommend the use of ACE-FTS to derive tropical upwelling velocities but we include this case merely as an illustrative example.

Figure 13 (top) shows the vertical velocities averaged over 60-30 hPa derived using raw model fields as well as the satellite-sampled data. To quantify the impact of the different orbital sampling patterns, Figure 13 (bottom) displays scatter plots between the raw fields and the satellite-sampled vertical velocities. The best correlation (R = 1.00), the best line fit (1.07x+0.02, obtained using an ordinary least squares fit regression) and the smallest RMSd (0.005) are found when using the MLS sampling. ACE-FTS and HALOE sampling lead to non-negligible artifacts when deriving vertical velocities from the tape recorder.

Previous studies have shown variability in middle stratospheric tropical vertical velocities on the order of up to ± 40% associated with the QBO and ENSO (Flury et al., 2013; Neu et al., 2014; Minschwaner et al., 2016). To better understand the impact of these sampling-induced artifacts, we fit the following model to the monthly vertical velocities

$$\mathrm{w_{TR}} = q * \mathrm{QSI}[t - t_q] + e * \mathrm{MEI}[t - t_e] + c \tag{10}$$

where $\mathrm{w_{TR}}$ is the vertical velocity derived from the tape recorder, QSI is a QBO shear index, MEI is the multivariate ENSO index, c is a baseline constant, q and e are constants modifying the magnitude of the QSI or MEI, and, t_q and t_e are the QSI or MEI time offsets, respectively. The QSI is calculated from the difference in the Singapore zonal winds at 50 and 25 hPa (Naujokat, 1986). The MEI is determined using a combination of the principal component analysis of sea level pressure, sea surface temperature, zonal and meridional surface winds, surface air temperature and cloudiness as described by Wolter et al. (1998, 2011). Figure 14(a) shows the time series of the QSI and the MEI, along with the vertical velocities averaged over 60-30 hPa derived using raw model fields. As can be seen, these vertical velocities are clearly correlated with the QSI but also show a strong relationship with the MEI in some years. Figure 14(b-e) displays the results of fitting the model described by equation 10 to the raw (b) and satellite-sampled (c-e) derived vertical velocities. The time offsets were fitted using the raw model fields and then imposed onto the satellite-sampled data. We do not fit a modeled seasonal cycle, such as the one described by equation 5, because the methodology used suppresses the seasonal cycle (Flury et al., 2013). As shown, this model is able to capture most of the variability in the derived vertical velocities. The fits are primarily driven by the QSI, with MLS sampling overestimating its influence by 3.8% (the differences in q in the equations shown in Figure 14), while HALOE and ACE-FTS sampling underestimate it by 30.7 and 31.5%, respectively. The impact of the sampling is more pronounced for the MEI (the differences in e), with MLS, HALOE and ACE-FTS underestimating its influence by 11, 64 and 122%. We emphasize that these sampling-induced offsets to the strength of the modulation effects of the QBO and ENSO on the circulation are only applicable to CMAM30-SD fields. These fields may not accurately represent the stratospheric tropical vertical velocities and, consequently, the actual sampling offsets could be different. As such, they should be considered only as potential biases.

The changes in tropical upwelling associated with QBO and ENSO assessed here have been shown to alter O_3 transport to the midlatitude lower stratosphere and to account for approximately half the interannual variability in midlatitude tropospheric O_3 (Neu et al., 2014). It has been hypothesized that this observed relationship between stratospheric upwelling changes and changes in tropospheric O_3 may provide an emergent constraint on the tropospheric O_3 response to long-term strengthening of the circulation associated with greenhouse gas increases. If so, accurate quantification of the variability in tropical vertical velocities is crucial to reducing uncertainties in estimating this response.

6 Summary

In this paper we evaluate the effect of orbital sampling on satellite measurements of stratospheric temperature and several trace gases. In particular, we quantify the impact of sampling in terms of the sampling bias. To illustrate the impact of orbital sampling on the outcome of representative atmospheric studies, we also quantify the induced differences in the inferred magnitude of trends and their detectability, as well as the induced differences in derived tropical vertical velocities. We calculate these sampling-induced artifacts by interpolating CMAM30-SD model fields (used as a proxy for the real atmosphere) to the real sampling patterns of three satellite instruments —Aura MLS, HALOE and ACE-FTS— to allow us to compare a dense uniform sampling pattern characteristic of limb emission sounders to the coarse non-uniform sampling patterns characteristic of solar occultation instruments.

The results suggest that overall:

- Coarse non-uniform sampling patterns, such as the ones from HALOE and ACE-FTS, can introduce sampling biases about an order of magnitude greater than those from dense uniform sampling patterns, such as the one from MLS. For example, we found a temperature maximum sampling bias of about 10 K compared to 1 K, and H_2O maximum sampling biases as large as 5% as opposed to less than 1%, in the middle stratosphere. These results corroborate the results of Toohey et al. (2013) and Sofieva et al. (2014).

- Dense uniform sampling patterns accurately reproduce the magnitude of the model trends with only small errors. Records based on such sampling patterns will require the same number of years as when using the raw model fields, that is to say, trend detection is limited only by the natural variability. In contrast, coarse non-uniform sampling patterns may introduce non-negligible errors in the inferred magnitude of trends, with considerably more years of data thus required to conclusively detect a given trend. This is because the sparse non-uniform sampling leads to an increase in the standard deviation of the total noise in the time series. For example, for near-global temperature trends (60°S-60°N) at 10 hPa, HALOE and ACE-FTS sampling patterns artificially bias the trend estimates by about -10 and 25%, respectively. Also, at 1 hPa, the pressure level where the strongest temperature trend was found in CMAM30-SD, an MLS sampling pattern will require 15 years to detect this particular trend, while the HALOE and ACE-FTS sampling will require 25 and 30 years, respectively.

- Coarse non-uniform sampling patterns may lead to an over or underestimation of the modulation effects of the controlling mechanisms of the tropical vertical velocities. For example, with respect to CMAM30-SD estimates, HALOE and ACE-FTS sampling patterns underestimate the QBO modulation strength by 30.7 and 31.5%, and the ENSO modulation strength by 64 and 122%, respectively. Dense uniform sampling patterns are considerably better suited to deriving tropical vertical velocities; for example, MLS sampling only overestimates the QBO influence by 3.8% and underestimates the ENSO influence by 11%.

Stratospheric changes such as a possible increase in the circulation and trends in temperature and O_3 are signatures of greenhouse gas warming and stratospheric O_3 recovery. Thus, our ability to accurately measure these changes is crucial for detecting anthropogenic influences on climate.

Acknowledgements. Work at the Jet Propulsion Laboratory, California Institute of Technology, was done under contract with the National Aeronautics and Space Administration. We thank David Plummer of Environment Canada for his assistance in obtaining the CMAM30-SD dataset.

References

Aghedo, A. M., Bowman, K. W., Shindell, D. T., and Faluvegi, G.: The impact of orbital sampling, monthly averaging and vertical resolution on climate chemistry model evaluation with satellite observations, Atmos. Chem. Phys., 11, 6493-6514, doi:10.5194/acp-11-6493-2011, 2011.

Beagley, S.R., de Grandpre, J., Koshyk, J. N., McFarlane, N.A.: Radiative dynamical climatology of the first generation Canadian middle atmosphere model, Atmosphere-Ocean, 35, 3, doi:10.1080/07055900.1997.9649595, 1997.

Bell, T. L., and Kundu, P. S.: A Study of the Sampling Error in Satellite Rainfall Estimates Using Optimal Averaging of Data and a Stochastic Model, J. Climate, 1251–1268, doi:10.1175/1520-0442(1996)009<1251:ASOTSE>2.0.CO;2, 1995.

Bernath, P. F., McElroy, C. T., Abrams, M. C., Boone, C. D., Butler, M., Camy-Peyret, C., Carleer, M., Clerbaux, C., Coheur, P.-F., Colin, R., DeCola, P., DeMazière, M., Drummond, J. R., Dufour, D., Evans, W. F. J., Fast, H., Fussen, D., Gilbert, K., Jennings, D. E., Llewellyn, E. J., Lowe, R. P., Mahieu, E., McConnell, J. C., McHugh, M., McLeod, S. D., Michaud, R., Midwinter, C., Nassar, R., Nichitiu, F., Nowlan, C., Rinsland, C. P., Rochon, Y. J., Rowlands, N., Semeniuk, K., Simon, P., Skelton, R., Sloan, J. J., Soucy, M.-A., Strong, K., Tremblay, P., Turnbull, D., Walker, K. A., Walkty, I., Wardle, D. A., Wehrle, V., Zander, R., Zou, J.: Atmospheric Chemistry Experiment (ACE): Mission overview, Geophys. Res. Lett., 32, L15S01, doi:10.1029/2005GL022386, 2005.

Boers, R., and van Meijgaard, E.: What are the demands on an observational program to detect trends in upper tropospheric water vapor anticipated in the 21st century? Geophys. Res. Lett., 36, L19806, doi:10.1029/2009GL040044, 2009.

Brindley, H. E. and Harries, J. E.: Observations of the Infrared Outgoing Spectrum of the Earth from Space: The Effects of Temporal and Spatial Sampling, J. Climate, 3820–3833, doi:10.1175/1520-0442(2003)016<3820:OOTIOS>2.0.CO;2, 2003.

Brühl, C., Drayson, S. R., Russell, J. M., Crutzen, P. J., McInerney, J. M., Purcell, P. N., Claude, H., Gernandt, H., McGee, T. J., McDermid, I. S., Gunson, M. R.: Halogen Occultation Experiment ozone channel validation, J. Geophys. Res., 101(D6), 10217–10240, doi:10.1029/95JD02031, 1996.

Clerbaux, C., Coheur,P.-F., Hurtmans, D., Barret, B., Carleer, M., Colin, R., Semeniuk, K., McConnell, J. C., Boone, C., and Bernath, P.: Carbon monoxide distribution from the ACE-FTS solar occultation measurements, Geophys. Res. Lett., 32, L16S01, doi:10.1029/2005GL022394, 2005.

Dee, D. P., Uppala, S. M., Simmons, A. J., Berrisford, P., Poli, P., Kobayashi, S., Andrae, U., Balmaseda, M. A., Balsamo, G., Bauer, P., Bechtold, P., Beljaars, A. C. M., van de Berg, L., Bidlot, J., Bormann, N., Delsol, C., Dragani, R., Fuentes, M., Geer, A. J., Haimberger, L., Healy, S. B., Hersbach, H., Hólm, E. V., Isaksen, L., Kållberg, P., Köhler, M., Matricardi, M., McNally, A. P., Monge-Sanz, B. M., Morcrette, J.-J., Park, B.-K., Peubey, C., de Rosnay, P., Tavolato, C., Thépaut, J.-N. and Vitart, F.: The ERA-Interim reanalysis: Configuration and performance of the data assimilation system. Q. J. R. Meteorol. Soc. 137, 553–597, 2011.

Dupuy, E., Walker, K. A., Kar, J., Boone, C. D., McElroy, C. T., Bernath, P. F., Drummond, J. R., Skelton, R., McLeod, S. D., Hughes, R. C., Nowlan, C. R., Dufour, D. G., Zou, J., Nichitiu, F., Strong, K., Baron, P., Bevilacqua, R. M., Blumenstock, T., Bodeker, G. E., Borsdorff, T., Bourassa, A. E., Bovensmann, H., Boyd, I. S., Bracher, A., Brogniez, C., Burrows, J. P., Catoire, V., Ceccherini, S., Chabrillat, S., Christensen, T., Coffey, M. T., Cortesi, U., Davies, J., De Clercq, C., Degenstein, D. A., De Mazière, M., Demoulin, P., Dodion, J., Firanski, B., Fischer, H., Forbes, G., Froidevaux, L., Fussen, D., Gerard, P., Godin-Beekmann, S., Goutail, F., Granville, J., Griffith, D., Haley, C. S., Hannigan, J. W., Höpfner, M., Jin, J. J., Jones, A., Jones, N. B., Jucks, K., Kagawa, A., Kasai, Y., Kerzenmacher, T. E., Kleinböhl, A., Klekociuk, A. R., Kramer, I., Küllmann, H., Kuttippurath, J., Kyrölä, E., Lambert, J.-C., Livesey, N. J., Llewellyn, E. J., Lloyd, N. D., Mahieu, E., Manney, G. L., Marshall, B. T., McConnell, J. C., McCormick, M. P., McDermid, I. S., McHugh, M., McLinden,

C. A., Mellqvist, J., Mizutani, K., Murayama, Y., Murtagh, D. P., Oelhaf, H., Parrish, A., Petelina, S. V., Piccolo, C., Pommereau, J.-P., Randall, C. E., Robert, C., Roth, C., Schneider, M., Senten, C., Steck, T., Strandberg, A., Strawbridge, K. B., Sussmann, R., Swart, D. P. J., Tarasick, D. W., Taylor, J. R., Tétard, C., Thomason, L. W., Thompson, A. M., Tully, M. B., Urban, J., Vanhellemont, F., Vigouroux, C., von Clarmann, T., von der Gathen, P., von Savigny, C., Waters, J. W., Witte, J. C., Wolff, M., and Zawodny, J. M.: Validation of ozone measurements from the Atmospheric Chemistry Experiment (ACE), Atmos. Chem. Phys., 9, 287-343, doi:10.5194/acp-9-287-2009, 2009.

Engelen, R. J., Fowler, L. D, Gleckler, P. J. and Wehner M. F.: Sampling strategies for the comparison of climate model calculated and satellite observed brightness temperatures, J. Geophys. Res., 105(D7), 9393–9406, doi:10.1029/1999JD901182, 2000.

Eyring et al.: Assessment of temperature, trace species, and ozone in chemistry climate model simulations of the recent past, J. Geophys. Res., 111 , D22308, doi:10.1029/2006JD007327, 2006.

Flury, T., Wu, D. L., and Read, W. G.: Correlation among cirrus ice content, water vapor and temperature in the TTL as observed by CALIPSO and Aura/MLS, Atmos. Chem. Phys., 12, 683-691, doi:10.5194/acp-12-683-2012, 2012.

Flury, T., Wu, D. L., and Read, W. G.: Variability in the speed of the Brewer–Dobson circulation as observed by Aura/MLS, Atmos. Chem. Phys., 13, 4563-4575, doi:10.5194/acp-13-4563-2013, 2013.

Gebremichael M. and Krajewski W. F.: Effect of Temporal Sampling on Inferred Rainfall Spatial Statistics, J. Applied Meteorol., 1626–1633, doi:10.1175/JAM2283.1, 2005.

de Grandpré, J., S. R. Beagley, V. I. Fomichev, E. Griffioen, J. C. McConnell, A. S. Medvedev, and T. G. Shepherd: Ozone climatology using interactive chemistry: Results from the Canadian Middle Atmosphere Model, Geophys. Res., 105, 26,475-26, 491, 2000.

Guan, B., Waliser, D. E., Li, J. F., and da Silva A.:, Evaluating the impact of orbital sampling on satellite–climate model comparisons, J. Geophys. Res. Atmos., 118, 355–369, doi:10.1029/2012JD018590, 2013.

Hegglin, M. I. and Shepherd, T. G.: O_3-N_2O correlations from the Atmospheric Chemistry Experiment: Revisiting a diagnostic of transport and chemistry in the stratosphere, J. Geoph. Res., 112, D19301, doi:10.1029/2006JD008281, 2007.

Hegglin, M. I. Plummer, D. A., Shepherd, T. G., Scinocca, J. F., Anderson, J., Froidevaux, L., Funke, B., Hurst, D., Rozanov, A., Urban, J., von Clarmann, T., Walker, K. A., Wang, H. J., Tegtmeier S., and Weigel, K.: Vertical structure of stratospheric water vapour trends derived from merged satellite data, Nature Geoscience, 7, 768–776, doi:10.1038/ngeo2236, 2014.

Hervig, M. E., Russell, J. M., Gordley, L. L., Drayson, S. R., Stone, K., Thompson, R. E., Gelman, M. E., McDermid, I. S., Hauchecorne, A., Keckhut, P., McGee, T. J., Singh, U. N., Gross, M. R.: Validation of temperature measurements from the Halogen Occultation Experiment, J. Geophys. Res., 101(D6), 10277–10285, doi:10.1029/95JD01713, 1996.

Jiang, J. H., Su, H., Zhai, C., Wu, L., Minschwaner, K., Molod, A. M., and Tompkins, A. M.: An assessment of upper troposphere and lower stratosphere water vapor in MERRA, MERRA2, and ECMWF reanalyses using Aura MLS observations, J. Geophys. Res. Atmos., 120 , 11,468–11,485, doi:10.1002/2015JD023752, 2015.

Jin, J. J., Semeniuk, K., Jonsson, A. I., Beagley, S. R., McConnel, J. C., Boone, C. D., Walker, K. A., Bernath, P. F., Rinsland, C. P., Dupuy, E., Ricaud, P., De La Noe, J., Urban J. and Murtagh, D.: Co-located ACE-FTS and Odin/SMR stratospheric-mesospheric CO 2004 measurements and comparison with a GCM, Geophys. Res. Lett., 32, L15S03, doi:10.1029/2005GL022433, 2005.

Jin, J. J., Semeniuk, K., Beagley, S. R., Fomichev, V. I., Jonsson, A. I., McConnell, J. C., Urban, J., Murtagh, D., Manney, G. L., Boone, C. D., Bernath, P. F., Walker, K. A., Barret, B., Ricaud, P., and Dupuy, E.: Comparison of CMAM simulations of carbon monoxide (CO), nitrous oxide (N2O), and methane (CH4) with observations from Odin/SMR, ACE-FTS, and Aura/MLS, Atmos. Chem. Phys., 9, 3233-3252, doi:10.5194/acp-9-3233-2009, 2009.

Livesey, N., Read, W. G., Wagner, P. A. Frovideaux, L., Lambert, A., Manney, G. L., Millan, L., Pumphrey, H. C., Santee, M. L., Schwartz, M. J., Wang, S., Fuller, R. A., Jarnot, R. F., Knosp, B. W., and Martinez, E.: Earth Observing System (EOS) Aura Microwave Limb Sounder (MLS) Version 4.2x Level 2 data quality and description document, JPL D-33509 Rev.A, JPL publication, USA, 2015.

Luo, M., Beer, R., Jacob, D. J., Logan, J. A., and Rodgers, C. D.: Simulated observation of tropospheric ozone and CO with the Tropospheric Emission Spectrometer (TES) satellite instrument, J. Geophys. Res., 107(D15), doi:10.1029/2001JD000804, 2002.

Manney, G. L., Daffer, W. H., Zawodny, J. M., Bernath, P. F., Hoppel, K. W., Walker, K. A., Knosp, B. W., Boone, C., Remsberg, E. E., Santee, M. L., Harvey, V. L., Pawson, S., Jackson, D. R., Deaver, L., McElroy, C. T., McLinden, C. A., Drummond, J. R., Pumphrey, H. C., Lambert, A., Schwartz, M. J., Froidevaux, L., McLeod, S., Takacs, L. L., Suarez, M. J., Trepte, C. R., Cuddy, S. C., Livesey, N. J., Harwood, R. S. and Waters, J. W.: Solar occultation satellite data and derived meteorological products: Sampling issues and comparisons with Aura Microwave Limb Sounder, J. Geophys. Res., 112, D24S50, doi:10.1029/2007JD008709, 2007.

McConnell, A., and North, G. R.: Sampling errors in satellite estimates of tropical rain, J. Geophys. Res., 92(D8), 9567–9570, doi:10.1029/JD092iD08p09567, 1987.

McLandress, C., Plummer, D. A., and Shepherd, T. G.: Technical Note: A simple procedure for removing temporal discontinuities in ERA-Interim upper stratospheric temperatures for use in nudged chemistry-climate model simulations, Atmos. Chem. Phys., 14, 1547-1555, doi:10.5194/acp-14-1547-2014, 2014.

Melo, S. M. L., Blatherwick, R., Davies, J., Fogal, P., de Grandpré, J., McConnell, J., McElroy, C. T., McLandress, C., Murcray, F. J., Olson, J. R., Semeniuk, K., Shepherd, T. G., Strong, K., Tarasick, D., and Williams-Rioux, B. J.: Summertime stratospheric processes at northern mid-latitudes: comparisons between MANTRA balloon measurements and the Canadian Middle Atmosphere Model, Atmos. Chem. Phys., 8, 2057-2071, doi:10.5194/acp-8-2057-2008, 2008.

Minschwaner, K., Su, H., and Jiang, J. H.:The upward branch of the Brewer-Dobson circulation quantified by tropical stratospheric water vapor and carbon monoxide measurements from the Aura Microwave Limb Sounder, J. Geophys. Res. Atmos., 121, doi:10.1002/2015JD023961, 2016

Naujokat, B.: An Update of the Observed Quasi-Biennial Oscillation of the Stratospheric Winds over the Tropics, J. Atmos. Sci., 43, 1873–1877, doi:10.1175/1520-0469(1986)043<1873:AUOTOQ>2.0.CO;2, 1986.

Neu, J. L., Flury, T., Manney, G. L., Santee, M. L., Livesey, N. J., and Worden J.: Tropospheric ozone variations governed by changes in stratospheric circulation, Nature Geoscience, 7, 340–344, doi:10.1038/ngeo2138, 2014.

Niwano, M., Yamazaki, K., and Shiotani M.: Seasonal and QBO variations of ascent rate in the tropical lower stratosphere as inferred from UARS HALOE trace gas data, J. Geophys. Res., 108, 4794, D24, doi:10.1029/2003JD003871, 2003.

North, G. R., Shen, S. S., and Upson R.: Sampling Errors in Rainfall Estimates by Multiple Satellites, J. Appl. Meteor, 32, 399–410, doi:10.1175/1520-0450(1993)032<0399:SEIREB>2.0.CO;2, 1993.

Pendlebury, D., Plummer, D., Scinocca, J., Sheese, P., Strong, K., Walker, K., and Degenstein, D.: Comparison of the CMAM30 data set with ACE-FTS and OSIRIS: polar regions, Atmos. Chem. Phys., 15, 12465-12485, doi:10.5194/acp-15-12465-2015, 2015.

Russell III, J. M., Gordley, L. L., Park, J. H., Drayson, S. R., Hesketh, W. D., Cicerone, R. J., Tuck, A. F., Frederick, J. E., Harries, J. E., and Crutzen, P. J.: The Halogen Occultation Experiment, J. Geophys. Res., 98(D6), 10777–10797, doi:10.1029/93JD00799, 1993.

Schoeberl, M. R., Douglass, A. R., Stolarski, R. S., Pawson, S., Strahan, S. E. and Read W.: Comparison of lower stratospheric tropical mean vertical velocities, J. Geophys. Res., 113, D24109, doi:10.1029/2008JD010221, 2008.

Shepherd, T. G., Plummer, D. A., Scinocca, J. F., Hegglin, M. I., Fioletov, V. E., Reader, M. C., Remsberg, E., von Clarmann, T., and Wang H. J.: Reconciliation of halogen-induced ozone loss with the total-column ozone record, Nature Geoscience, 7, 443–449, doi:10.1038/ngeo2155, 2014

Sica, R. J., Izawa, M. R. M., Walker, K. A., Boone, C., Petelina, S. V., Argall, P. S., Bernath, P., Burns, G. B., Catoire, V., Collins, R. L., Daffer, W. H., De Clercq, C., Fan, Z. Y., Firanski, B. J., French, W. J. R., Gerard, P., Gerding, M., Granville, J., Innis, J. L., Keckhut, P., Kerzenmacher, T., Klekociuk, A. R., Kyrö, E., Lambert, J. C., Llewellyn, E. J., Manney, G. L., McDermid, I. S., Mizutani, K., Murayama, Y., Piccolo, C., Raspollini, P., Ridolfi, M., Robert, C., Steinbrecht, W., Strawbridge, K. B., Strong, K., Stübi, R., and Thurairajah, B.: Validation of the Atmospheric Chemistry Experiment (ACE) version 2.2 temperature using ground-based and space-borne measurements, Atmos. Chem. Phys., 8, 35-62, doi:10.5194/acp-8-35-2008, 2008.

Sofieva, V. F., Kalakoski, N., Päivärinta, S.-M., Tamminen, E. Kyrölä J., Laine, M., and Froidevaux, L.: On sampling uncertainty of satellite ozone profile measurements, Atmos. Meas. Tech., 7, 1891-1900, doi:10.5194/amt-7-1891-2014, 2014.

Soman, V. V., Valdés, J. B. and North, G. R.:, Estimation of sampling errors and scale parameters using two- and three-dimensional rainfall data analyses, J. Geophys. Res., 101(D21), 26453–26460, doi:10.1029/96JD01387, 1996.

Taylor, K. E: Summarizing multiple aspects of model performance in a single diagram, J. Geoph. Res., vol 106, no. D7, 7183-7192, doi:10.1029/2000JD900719, 2001.

Tiao, G. C, Reinsel, G. C., Xu, D., Pedrick, J. H., Zhu, X., Miller, A. J., DeLuisi, J. J., Mateer, C. L., and Wuebbles, D. J.: Effects of autocorrelation and temporal sampling schemes on estimates of trend and spatial correlation, J. Geophys. Res., 95(D12), 20507–20517, doi:10.1029/JD095iD12p20507, 1990.

Toohey, M., Hegglin, M. I., Tegtmeier, S., Anderson, J., Añel, J. A., Bourassa, A., Brohede, S., Degenstein, D., Froidevaux, L., Fuller, R., Funke, B., Gille, J., Jones, A., Kasai, Y., Krüger, K., Kyrölä, E., Neu, J. L., Rozanov, A., Smith, L., Urban, J., von Clarmann, T., Walker, K. A. and Wang, R. H. J.: Characterizing sampling biases in the trace gas climatologies of the SPARC Data Initiative, J. Geophys. Res. Atmos., 118, 11,847–11,862, doi:10.1002/jgrd.50874, 2013.

Weatherhead, E. C., Reinsel, G. C., Tiao, G. C., Meng, X. L., Choi, D., Cheang, W. K., Keller, T., DeLuisi, J., Wuebbles, D. J., Kerr, J. B., Miller, A. J., Oltmans, S. J., and Frederick J. E.: Factors affecting the detection of trends: Statistical considerations and applications to environmental data, J. Geophys. Res., 103(D14), 17149–17161, doi:10.1029/98JD00995, 1998.

Whiteman, D. N., Vermeesch, K. C., Oman, L. D. and Weatherhead, E. C.: The relative importance of random error and observation frequency in detecting trends in upper tropospheric water vapor, J. Geophys. Res., 116, D21118, doi:10.1029/2011JD016610, 2011.

Wolter, K., and Timlin, M. S.: Measuring the strength of ENSO events - how does 1997/98 rank? Weather, 53, 315–324, doi:10.1002/j.1477-8696.1998.tb06408.x, 1998.

Wolter, K., and Timlin, M. S.: El Niño/Southern Oscillation behaviour since 1871 as diagnosed in an extended multivariate ENSO index (MEI.ext). Intl. J. Climatology, 31, 1074-1087, doi:10.1002/joc.2336, 2011.

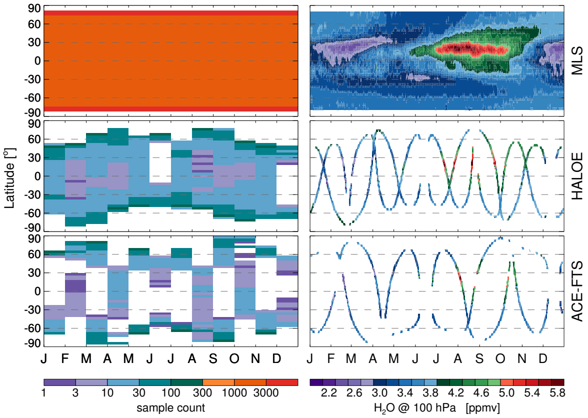

Figure 1. (left) Monthly sampling counts for MLS, HALOE and ACE-FTS, in 4° latitude bins. Note the non-uniform colorbar increments. (right) Zonal mean water vapor at 100 hPa as sampled by MLS, HALOE and ACE-FTS for individual days. White regions denote a lack of measurements.

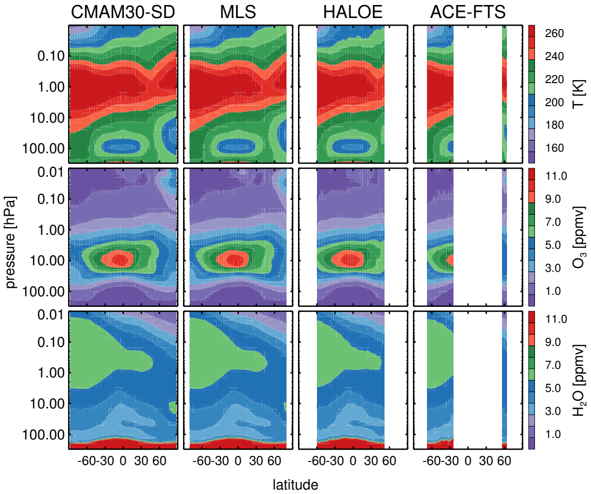

Figure 2. January 2005 zonal means as a function of pressure for temperature, O_3 and H_2O (top to bottom) in 4° latitude bins. Left column is raw CMAM30-SD model fields, other columns are CMAM30-SD as sampled by MLS, HALOE and ACE-FTS (left to right), respectively. White regions denote a lack of measurements.

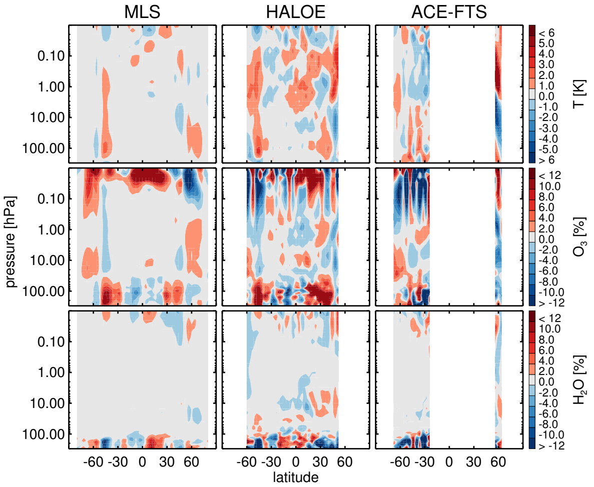

Figure 3. January 2005 sampling bias as a function of latitude and pressure for temperature, O_3, and H_2O (top to bottom) as measured using MLS, HALOE and ACE-FTS sampling patterns (left to right). White regions denote a lack of measurements.

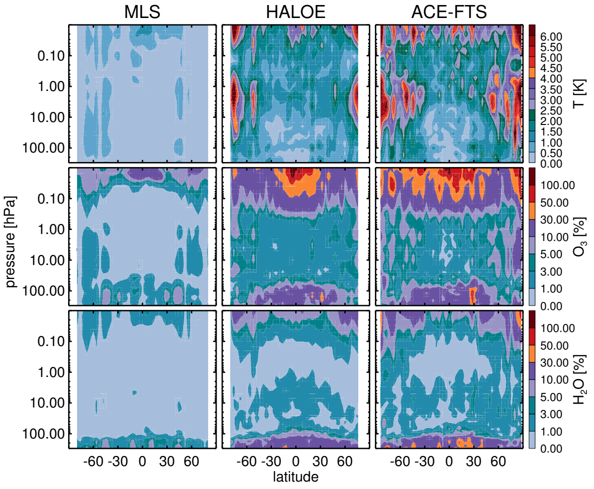

Figure 4. Root mean square sampling bias for 2005 as a function of latitude and pressure for temperature, O_3, and H_2O (top to bottom) as measured using MLS, HALOE and ACE-FTS sampling patterns (left to right). White regions denote a lack of measurements.

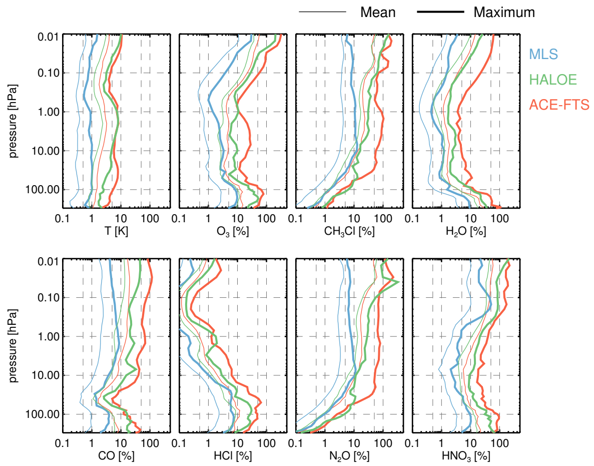

Figure 5. Mean (thin lines) and maximum (thicker lines) RMS sampling bias over all latitudes for 2005 as a function of pressure for temperature (in Kelvin), O_3, CH_3Cl, H_2O, CO, HCl, N_2O and HNO_3 in %. The vertical grid indicates values of 0.5, 1, 5, 10, 50, 100.

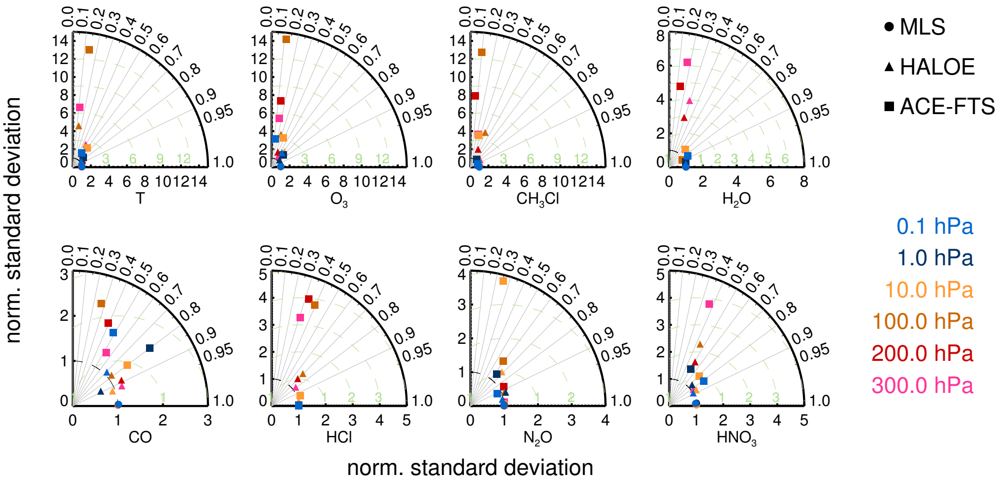

Figure 6. Taylor diagrams showing near-global (60°S to 60°N) long-term (1979–2012) pattern comparisons between the raw (the reference point at (1,0)) and the satellite-sampled data at different pressure levels. The green contours indicate the normalized RMS difference values.

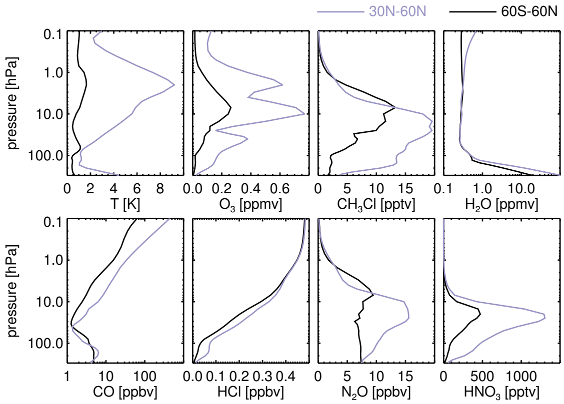

Figure 7. Raw model standard deviations used to normalize the Taylor diagrams shown in Figure 6 and in Figure 10. Note that H_2O and CO are shown using a logarithmic scale.

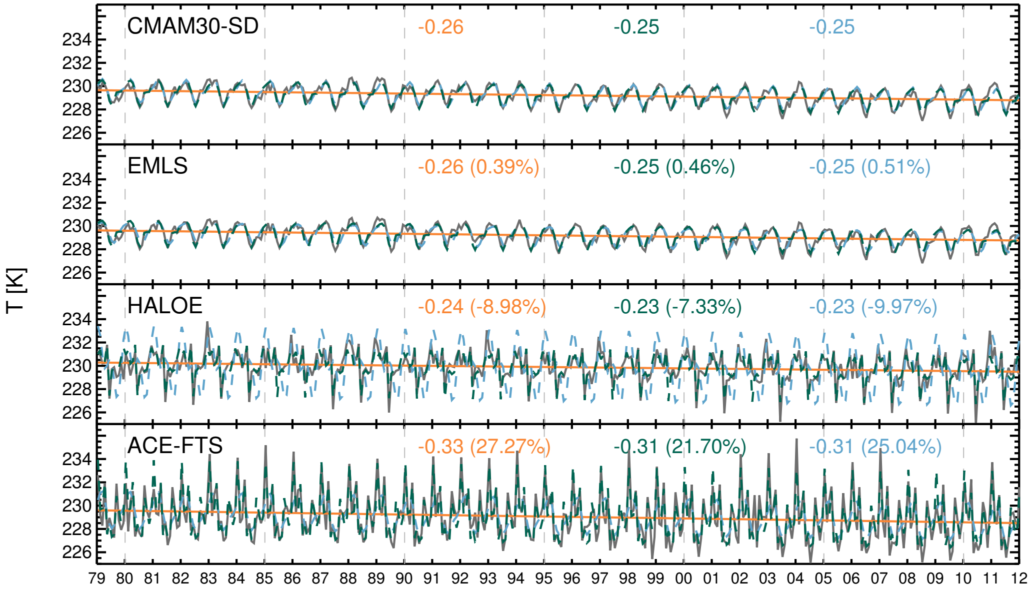

Figure 8. Time series of near-global (60°S to 60°N) temperature at 10 hPa for the raw and satellite-sampled data (gray lines). Orange lines display the trend computed using the linear fit, green lines show the climatological seasonal cycle imposed upon a long-term trend and light blue lines show the model computed using equation 4. The trend (K decade^{-1}) computed using each method is specified in each subplot; in brackets we show the percentage difference in trend magnitude with respect to the trend found using the raw model data.

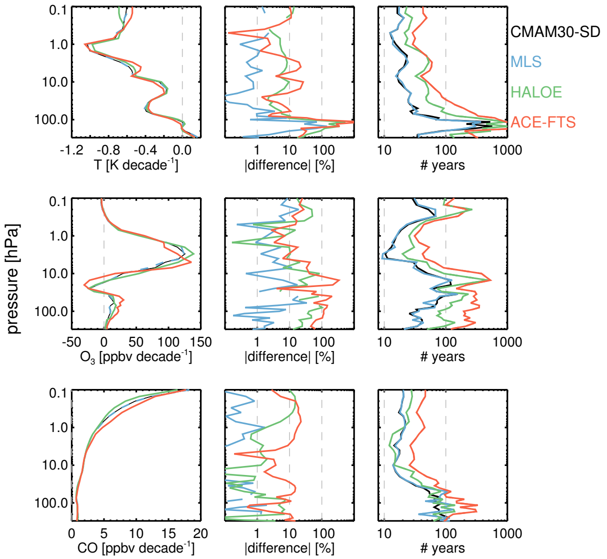

Figure 9. (left) Near-global (60°S to 60°N) long-term (1979–2012) trends computed using equation 4 for temperature, O$_3$ and CO. (middle) Percentage difference in the inferred magnitude of the trends when computed using various satellite-sampled data with respect to the one computed using the raw model fields. (right) Number of years required to detect such trends.

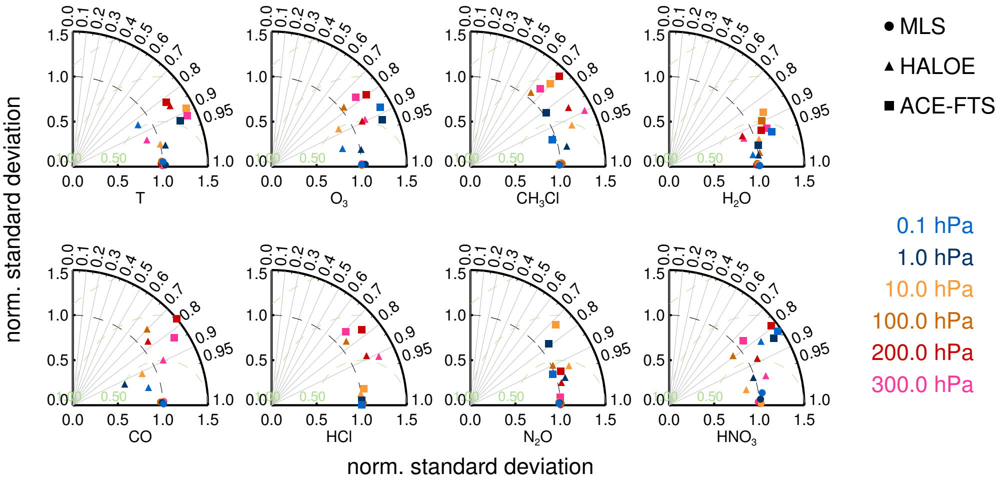

Figure 10. As figure 6 but for 30°N to 60°N.

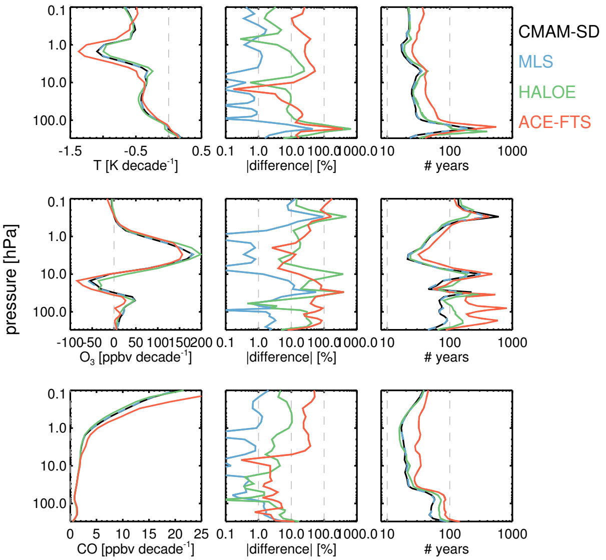

Figure 11. As figure 9 but for 30°N to 60°N.

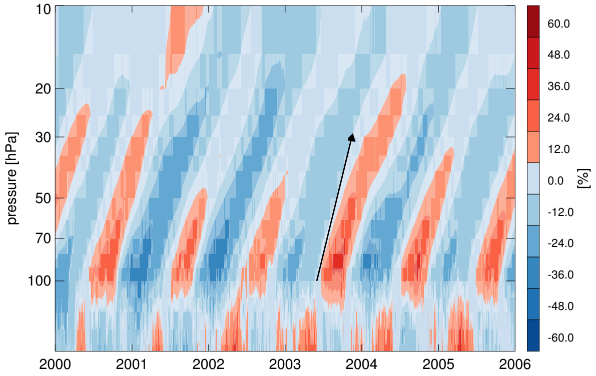

Figure 12. The atmospheric tape recorder (zonal mean water vapor anomalies in the tropics, in this case for CMAM30-SD raw model fields) displays a clear signal of the large-scale upward transport as indicated by the arrow. The slope of this arrow, which is derived from the propagation speed of the water vapor anomalies, represents the average tropical upwelling velocity for 8°S-8°N. This subset of years is shown as an example; other years are similar.

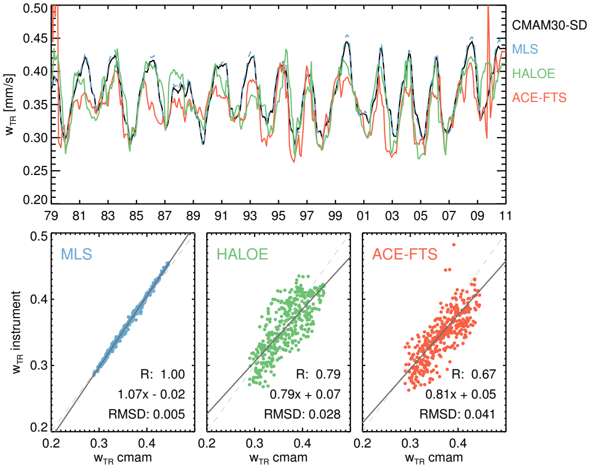

Figure 13. (top) w_{TR} (monthly vertical velocities) derived using daily time-correlations of the water vapor tape recorder at different pressure levels from the raw CMAM30-SD data as well as the satellite-sampled data. w_{TR} derived using the raw model fields and MLS-sampled data are almost identical. The pressure levels averaged are 30, 40, 50 and 60 hPa. (bottom) w_{TR} scatterplots [mm/s] for MLS, HALOE and ACE-FTS sampling, respectively, versus the velocities derived using raw model fields. The slopes' 95% confidence intervals are ± 0.007, 0.06 and 0.09 for MLS, HALOE and ACE-FTS, respectively.

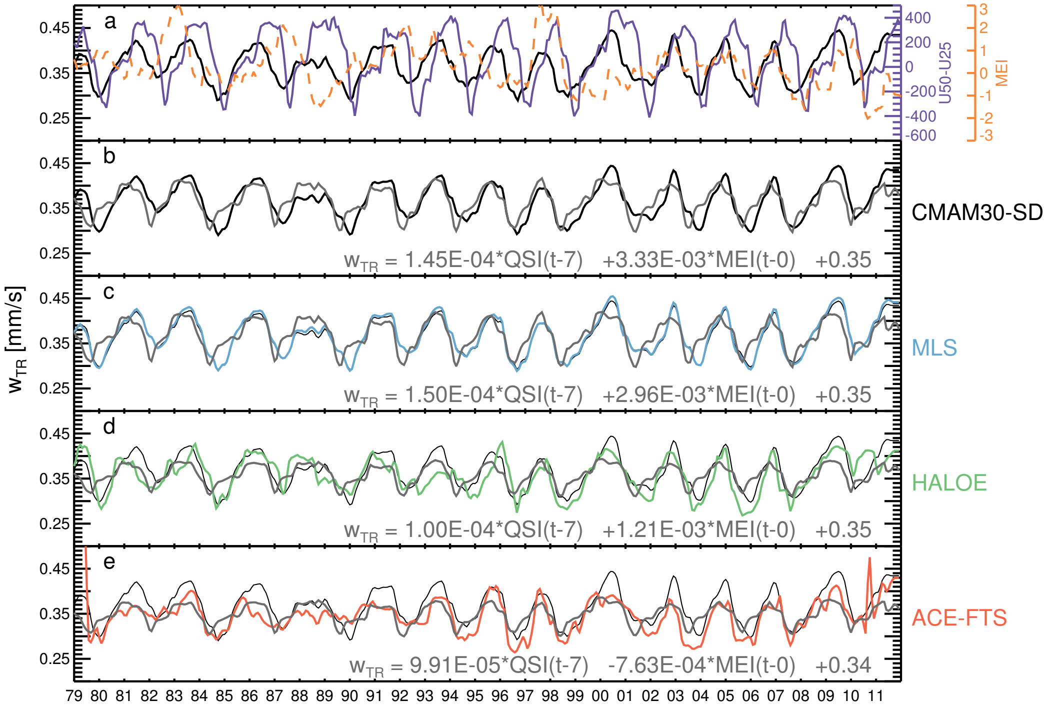

Figure 14. (a) Time series of w_{TR} (mean monthly vertical velocities averaged over 30, 40, 50 and 60 hPa) derived using CMAM30-SD raw data (black), the quasibiennial oscillation (QBO) shear index (QSI - purple) and the Multivariate ENSO index (MEI - orange dashed line). (b) Time series of w_{TR} for the raw model fields (black) as well as the model fit described by equation 10 (gray). (c-e) Time series of w_{TR} for satellite-sampled data (color coded). The thin black line displays the same w_{TR} derived using raw model fields (black line in panel b) for ease of comparison with the satellite-sampled ones. The model fit for each of the satellite-sampled w_{TR} values, described by equation 10, is shown in gray for each of these time series.